Dynamics of positrons during relativistic electron runaway

O. Embréus[1]†, L. Hesslow[1], M. Hoppe[1], G. Papp[2], K. Richards[1] and T. Fülöp[1]

[1]Department of Physics, Chalmers University of Technology, SE-41296 Göteborg, Sweden
[2]Max-Planck-Institute for Plasma Physics, Garching, Germany

(Received xx; revised xx; accepted xx)

Sufficiently strong electric fields in plasmas can accelerate charged particles to relativistic energies. In this paper we describe the dynamics of positrons accelerated in such electric fields, and calculate the fraction of created positrons that become runaway accelerated, along with the amount of radiation that they emit. We derive an analytical formula that shows the relative importance of the different positron production processes, and show that above a certain threshold electric field the pair production by photons is lower than that by collisions. We furthermore present analytical and numerical solutions to the positron kinetic equation; these are applied to calculate the fraction of positrons that become accelerated or thermalized, which enters into rate equations that describe the evolution of the density of the slow and fast positron populations. Finally, to indicate operational parameters required for positron detection during runaway in tokamak discharges, we give expressions for the parameter dependencies of detected annihilation radiation compared to bremsstrahlung detected at an angle perpendicular to the direction of runaway acceleration. Using the full leading order pair production cross section, we demonstrate that previous related work has overestimated the collisional pair production by at least a factor of four.

1. Introduction

The production of positrons has been investigated extensively both theoretically and experimentally since their first identification (Anderson 1932). Low energy positrons are used in many areas of science and technology, ranging from positron emission tomography (Raichle 1985) and surface science (Hunt *et al.* 1999) to fundamental studies of antimatter (Gabrielse *et al.* 2002; Surko & Greaves 2004). High energy positrons can also be routinely produced in particle accelerators and intense laser-solid interactions (Chen *et al.* 2009; Sarri 2015). Positrons are present in a wide range of atmospheric and astrophysical plasmas, e.g. lightning discharges (Dwyer & Uman 2014), solar flares (Murphy *et al.* 2005), pulsars and black-hole physics (Prantzos *et al.* 2011). Also in post-disruption plasmas in large tokamaks, where the energy of the runaway electrons is in the tens of MeV range, high-energy positrons should be present (Helander & Ward 2003; Fülöp & Papp 2012), but they have not yet been experimentally observed.

Plasmas with strong electric fields are particularly interesting for positron generation, as particles accelerated by the field often reach energies larger than the pair-production threshold. For example, the electric field in solar flares is believed to be the result of magnetic reconnection (Priest & Forbes 2002; Liu & Wang 2009). In thunderstorms strong electric fields are produced by the charged regions, sometimes lasting tens of minutes

† Email address for correspondence: embreus@chalmers.se

(Tsuchiya *et al.* 2011). In intense laser-matter interaction, the positrons experience the sheath field that is set up by the relativistic electrons leaving the target (Wilks *et al.* 2001). In disruptive tokamak plasmas, the resistivity increase due to the sudden cooling of the plasma leads to a high electric field that is induced to maintain the plasma current (Helander *et al.* 2002). Regardless of the cause, the electric field will strongly affect the dynamics of the positrons.

If the electric field exceeds a certain critical field, the accelerating force on the charged particles overcomes the friction, and they are accelerated to high energies and run away (Wilson 1925; Dreicer 1959). Existing runaway electrons may create new (secondary) runaways in close-collisions with thermal electrons, and this can lead to an exponential growth of the runaway population, i.e. an avalanche (Sokolov 1979; Rosenbluth & Putvinski 1997). The runaways are accelerated to energies that are well above the pair-production threshold (Hollmann *et al.* 2015; Paz-Soldan *et al.* 2017) and create positrons in collisions with electrons and ions. The created positrons are also accelerated by the electric field, in the opposite direction with respect to the electrons, and if the electric field is sufficiently strong, a substantial fraction of them will run away (Fülöp & Papp 2012). Eventually they will annihilate, either directly with electrons or through the formation of positronium (Charlton & Humberston 2001). Due to their drift motion, for runaway positrons in tokamaks this will typically occur after they have escaped the plasma and struck the first wall (Liu *et al.* 2014).

The direct annihilation of an electron-positron pair at rest will result in the creation of two gamma ray photons, each of energy 511 keV. Positron annihilation is often invoked to explain the observed emission features in the vicinity of 500 keV in the radiation spectrum of gamma-ray bursts, pulsars, solar flares (Murphy *et al.* 2005), terrestrial lightning (Briggs *et al.* 2011) and the galactic centre (Prantzos *et al.* 2011). In laboratory plasmas, the bremsstrahlung of the energetic electrons may overwhelm the annihilation radiation from the positrons, as the positron/electron fraction is usually low (Fülöp & Papp 2012). However, due to the directionality of the bremsstrahlung radiation, the isotropic annihilation radiation may still be detectable.

In this paper, we analyse the dynamics of high-energy positrons produced in collisions between charged particles in a strong electric field, where both electrons and positrons may run away. We use MadGraph 5 simulations (Alwall *et al.* 2014) to obtain the cross section for pair production in collisions between electrons and ions, which reveals that the high-energy limit (Landau & Lifshitz 1983) or the formula given in Gryaznykh (1998) significantly overestimates the cross section. We consider the relative importance of pair production by collisions and photons, and derive a critical pair-production field above which collisional pair production dominates in avalanching runaway scenarios.

In the case when pair production by photons is negligible, we solve the kinetic equation for positrons. We derive an analytical expression for the positron distribution function in the presence of an avalanching runaway electron population. The analytical results for the distribution function and critical electric field are corroborated with numerical simulations using the kinetic equation solver CODE (Landreman *et al.* 2014; Stahl *et al.* 2016) modified to include the positron source and annihilation terms. Furthermore, we consider the radiation emitted by positrons and find the parameter dependencies of the annihilation to bremsstrahlung radiation ratio. This allows determination of the parameter regions where the annihilation radiation could be detectable in these plasmas.

The structure of the paper is the following. In Sec. 2 we describe the kinetic equation of the positrons including details of the positron production source term. We present both analytical and numerical solutions of the kinetic equation, showing excellent agreement in the relevant limit. Following this, in Section 3 we describe rate equations for runaway

positrons, which are useful to predict the parametric dependencies of the fraction of positrons without extensive kinetic simulations. In Section 4 we calculate the expected annihilation radiation from positrons in tokamak plasmas. Finally we summarize our conclusions in Sec. 5.

2. Kinetic equation for positrons

In this paper we consider the dynamics of positrons during a relativistic electron runaway avalanche (Jayakumar *et al.* 1993). Due to the non-monotonic dynamical friction acting on a charged test particle in a plasma, in an electric field larger than a critical value E_c fast electrons may experience a net force that can rapidly accelerate them to energies in the range of tens of MeV. In a fully ionized plasma, the critical field is $E_c = \ln\Lambda n_e e^3/(4\pi\varepsilon_0^2 m_e c^2)$ (Connor & Hastie 1975), where $\ln\Lambda \approx 14.6 + 0.5\ln(T[\mathrm{eV}]/n_e[10^{20}\ \mathrm{m}^{-3}])$ is the Coulomb logarithm (Solodov & Betti 2008). We neglect a logarithmic energy dependence in $\ln\Lambda$, and use the value for relativistic electrons at 1 MeV for simplicity. Here, n_e is the electron density, e the elementary charge, ε_0 the vacuum permittivity, m_e the electron rest mass and c the speed of light. The background plasma is assumed to be nearly Maxwellian for all species with the same temperature T. In a neutral gas, $\ln\Lambda$ depends on the mean excitation energy of the medium instead of the temperature, and corresponds to $\ln\Lambda \approx 11$ in air (Gurevich & Zybin 2001). In this case the electron density refers to the density of bound electrons.

A sufficiently energetic electron can produce new runaway electrons through elastic large-angle collisions. The result is an exponentially growing number of runaway electrons, a so-called runaway *avalanche*. Each e-folding of the number density takes a time $t_{\mathrm{ava}} = c_Z/[4\pi n_e r_0^2 c(E/E_c - 1)]$ where c_Z is only weakly dependent on electric field, and can be approximated by $c_Z \approx \sqrt{5 + Z_{\mathrm{eff}}}$ in a fully ionized plasma (Rosenbluth & Putvinski 1997), where the effective charge is $Z_{\mathrm{eff}} = \sum n_i Z_i^2 / \sum_i n_i Z_i$ with the sum taken over all ion species i. We shall find that several results in the paper are insensitive to the details of c_Z, assuming only that it is independent of E. As such, more accurate models of the avalanche process can in principle be implemented by inserting for c_Z the value characterizing any particular scenario of interest.

Since the electrons are ultra-relativistic, they will create positrons which are predominantly co-moving; these are created either directly in collisions or indirectly through the hard X-rays emitted in collisions (Heitler 1954), which can produce a pair in a subsequent interaction. Since the positrons experience an acceleration by the electric field in the direction opposite to the runaway-electron motion, they will immediately start decelerating. A fraction of these positrons will slow down to thermal speeds where they eventually annihilate, whereas the remainder obtain sufficiently large momenta perpendicular to the acceleration direction that they become runaway-accelerated along the electric field, moving anti-parallel to the runaway electrons. Annihilation – which occurs at a rate that decreases with positron energy – does not have a significant effect on the dynamics of the energetic positrons since the avalanche rate is typically much faster, which is demonstrated in Sec. 2.2.

Throughout this paper, we shall assume that the plasma is fully ionized. In a partially ionized plasma or a neutral gas, screening effects due to the bound electrons would enter into all binary interactions. In the 10 MeV energy range, these are however largely negligible for the pair production mechanisms as well as for the emission of bremsstrahlung, meaning that they are to be calculated using the full nuclear charge of the target. The screening effects become significant when $p/m_e c \gtrsim 137/Z^{1/3}$ (Heitler 1954). Elastic Coulomb collisions are to a greater extent affected by screening effects,

where the pitch-angle scattering rates may be reduced by approximately up to two thirds and energy-loss rates by one third (Hesslow *et al.* 2017) in the energy range of interest, compared to the results obtained treating the medium as fully ionized. This would modify primarily two important quantities that affect our results: the avalanche growth rate factor c_Z, as well as the critical field E_c (Hesslow *et al.* 2018), which can here be assumed to be accurate only up to an order-of-unity factor in partially ionized plasmas. While the results we present are strictly valid for a fully ionized plasma, we expect to capture the correct order of magnitude also in a partially ionized plasma or neutral gas, if the effective charge and electron densities appearing in the formulas are always evaluated using the fully-ionized values. We denote these by

$$n_{\mathrm{tot}} = \sum_i Z_i n_i,$$
$$Z_{\mathrm{tot}} = \frac{1}{n_{\mathrm{tot}}} \sum_i n_i Z_i^2,$$

where Z_i is the atomic number of species i. Thus, the density is always to be taken as the total density of free plus bound electrons, and in a single-component gas or plasma Z_{tot} is the atomic number of the ion species regardless of ionization degree.

The dynamics described above can be most lucidly captured in a two-dimensional model. The distribution function of positrons with momentum $\boldsymbol{p} = m_e \boldsymbol{v}/\sqrt{1 - v^2/c^2}$, where the positron velocity is denoted $\boldsymbol{v}$, at a time t is denoted $f_{\mathrm{pos}}(t, \boldsymbol{p})$. In a homogeneous cylindrically symmetric plasma in the presence of an electric field $\boldsymbol{E}$ it satisfies the kinetic equation

$$\frac{\partial f_{\mathrm{pos}}}{\partial t} + eE\left[\xi \frac{\partial}{\partial p} + \frac{1-\xi^2}{p}\frac{\partial}{\partial \xi}\right] f_{\mathrm{pos}} = C_{\mathrm{pos}} + S_{\mathrm{pos}} + S_{\mathrm{an}}, \tag{2.1}$$

where $E = |\boldsymbol{E}|$, $p = |\boldsymbol{p}|$, $\xi \equiv \cos\theta = \boldsymbol{p}\cdot\boldsymbol{E}/pE$ is the pitch-angle cosine, C_{pos} is the positron collision operator, S_{pos} denotes the source term of positrons generated in collisions between relativistic runaway electrons and field particles of the plasma, as well as positron production by highly energetic photons, and S_{an} denotes the annihilation term. In a magnetized plasma, the equation is valid for an axisymmetric positron distribution if E is replaced by the component of the electric field parallel to the magnetic field, and the pitch angle is instead defined relative to the magnetic field.

In the limit of small energy transfers, the elastic positron-electron and positron-ion differential scattering cross sections coincide with the electron-electron and electron-ion cross sections, respectively (Landau & Lifshitz 1983). Consequently, the positron collision operator C_{pos} equals the electron collision operator C_e up to terms small in the Coulomb logarithm $\ln\Lambda$. Large-angle collisions, which are primarily important for avalanche generation when $\ln\Lambda$ is large, can be neglected since the thermal positron population will always be small in number. The positron distribution therefore satisfies the same kinetic equation as the electron distribution, except for the electric field accelerating them in the opposite direction (with these definitions positrons are accelerated towards $\xi = 1$, and electrons towards $\xi = -1$), and the presence of the terms S_{pos} and S_{an} describing their creation and annihilation, respectively.

The number of positrons created with momentum $\boldsymbol{p}$ in time $\mathrm{d}t$ has two main contributions: (*1*) the collisions between stationary ions of species i with density n_i and the $\mathrm{d}n_{\mathrm{RE}}$ number of runaways at momentum $\boldsymbol{p}_1$ and speed v_1, and (*2*) the pair production of $\mathrm{d}n_\gamma$ photons in the field of ions i:

$$\mathrm{d}n_{\mathrm{pos}} = \sum_i \left[n_i v_1 \mathrm{d}\sigma^+_{ci} \mathrm{d}n_{\mathrm{RE}} \mathrm{d}t + n_i c \mathrm{d}\sigma^+_{\gamma i} \mathrm{d}n_\gamma \mathrm{d}t \right]. \tag{2.2}$$

Here, $\mathrm{d}\sigma^+_{ci}$ is the differential cross section for producing a positron in a collision between an electron and a stationary ion, and similarly $\mathrm{d}\sigma^+_{\gamma i}$ for a photon interacting with stationary ions, and are given in Appendix A. We use the Madgraph 5 tool (Alwall *et al.* 2014) for obtaining the pair-production cross sections throughout this paper.

Using $\mathrm{d}n_{\mathrm{RE}}(\boldsymbol{p}_1) = f_{\mathrm{RE}}(\boldsymbol{p}_1)\mathrm{d}\boldsymbol{p}_1$, where f_{RE} is the distribution function of runaway electrons, and similarly for the positron distribution $f_{\mathrm{pos}}(\boldsymbol{p}) = \mathrm{d}n_{\mathrm{pos}}/\mathrm{d}\boldsymbol{p}$ and photons $\phi_\gamma(\boldsymbol{k}) = \mathrm{d}n_\gamma/\mathrm{d}\boldsymbol{k}$ where $\boldsymbol{k}/c$ is the photon momentum, we find the following form for the positron source S_{pos}:

$$S_{\mathrm{pos}} \equiv \left(\frac{\partial f_{\mathrm{pos}}}{\partial t} \right)_{\mathrm{pp}} = \sum_i n_i c \left[\int \mathrm{d}\boldsymbol{p}_1 \, \frac{v_1}{c} \frac{\partial \sigma^+_{ci}}{\partial \boldsymbol{p}} f_{\mathrm{RE}}(\boldsymbol{p}_1) + \int \mathrm{d}\boldsymbol{k} \, \frac{\partial \sigma^+_{\gamma i}}{\partial \boldsymbol{p}} \phi_\gamma(\boldsymbol{k}) \right]. \tag{2.3}$$

In an avalanching runaway scenario, the photon distribution can be eliminated in favour of an expression involving only the runaway distribution because of the relatively slow evolution of the photon energy spectrum. The runaway-electron population grows exponentially in time on the time-scale (Rosenbluth & Putvinski 1997)

$$t_{\mathrm{ava}} = \frac{c_Z}{4\pi n_{\mathrm{tot}} r_0^2 c (E/E_c - 1)}.$$

The photons on the other hand evolve on the Compton-scattering time scale (Heitler 1954)

$$t_{\mathrm{Co}} = \frac{k}{\pi n_{\mathrm{tot}} r_0^2 c m_e c^2 \ln\left[2k/(m_e c^2)\right]},$$

where the photon energies $k = |\boldsymbol{k}|$ are larger than the pair-production threshold $2m_e c^2$, and $r_0 = e^2/(4\pi\varepsilon_0 m_e c^2) \approx 2.82 \cdot 10^{-15}\,\mathrm{m}$ is the classical electron radius. Comparing the two time scales shows that the photons do not have time to change significantly from the distribution in which they are created whenever

$$\frac{k/m_e c^2}{\ln(2k/m_e c^2)} \gg \frac{c_Z}{4(E/E_c - 1)}.$$

Since the right-hand side is typically smaller than unity, this is generally well satisfied in an avalanching runaway scenario. The photon distribution is then given by

$$\phi(\boldsymbol{k}) = t_{\mathrm{ava}} \sum_i n_i \int \mathrm{d}\boldsymbol{p}_1 \, v_1 \frac{\partial \sigma_{\mathrm{br},i}}{\partial \boldsymbol{k}}(\boldsymbol{k}, \boldsymbol{p}_1) f_{\mathrm{RE}}(\boldsymbol{p}_1), \tag{2.4}$$

where $\mathrm{d}\sigma_{\mathrm{br},i}$ is the differential bremsstrahlung cross section for interactions between electrons and particle species i.

Since the cross sections appearing in these formulas depend on target species only through Z_i^2, the target charge squared (Heitler 1954), these may be factored out when screening effects are neglected, yielding a factor of the effective plasma charge Z_{tot} when summed over i. We shall therefore suppress the indices i of the cross sections by writing $\sum_i n_i \sigma^+_{ci} = n_{\mathrm{tot}} Z_{\mathrm{tot}} \sigma^+_c$ for collisional pair production, and $\sum_i n_i \sigma_{\mathrm{br},i} = n_{\mathrm{tot}}(Z_{\mathrm{tot}} + 1)\sigma_{\mathrm{br}}$ (and likewise for σ^+_γ) for the photon pair production cross sections. Here we have added the contribution from electron-electron bremsstrahlung in the approximation that the electron-electron and electron-proton bremsstrahlung cross sections are the same, which has satisfactory accuracy since the majority of interactions occur with negligible momentum transfer to the target particle (Haug 1975). Conversely, for collisional pair

production the electron-electron interactions are negligible, which was verified with MadGraph 5 simulations (Alwall *et al.* 2014; Ferretti 2018) which indicated that the *e-e* cross section is 10-20% of the *e-i* cross section when the incident electron lab-frame energy ranges over 10-20 MeV and $Z_i = 1$.

The positron source can then be written

$$S_{\rm pos} = Z_{\rm tot} n_{\rm tot} \int \mathrm{d}\boldsymbol{p}_1 \, v_1 \frac{\partial \sigma^+}{\partial \boldsymbol{p}} f_{\rm RE}(\boldsymbol{p}_1), \tag{2.5}$$

where the effective pair-production cross section $\mathrm{d}\sigma^+$, accounting for both direct pair production in collisions as well as by X-rays, is given by

$$\frac{\partial \sigma^+}{\partial \boldsymbol{p}} = \frac{\partial \sigma_c^+}{\partial \boldsymbol{p}} + \frac{(Z_{\rm tot}+1)^2}{Z_{\rm tot}} t_{\rm ava} n_{\rm tot} c \int \mathrm{d}\boldsymbol{k} \, \frac{\partial \sigma_\gamma^+}{\partial \boldsymbol{p}}(\boldsymbol{p}, \boldsymbol{k}) \frac{\partial \sigma_{\rm br}}{\partial \boldsymbol{k}}(\boldsymbol{k}, \boldsymbol{p}_1). \tag{2.6}$$

Positrons are created with a significant fraction of the energy of the incident electron that created them, but with a momentum perpendicular to the direction of the incident electron of order (Landau & Lifshitz 1983; Heitler 1954) $p_\perp \approx m_e c$. This means that the differential cross section for their production is strongly peaked in the direction of the incident electron; throughout this work we assume that it is delta distributed in the scattering angles, and write

$$\begin{aligned}
\frac{\partial \sigma_c^+}{\partial \boldsymbol{p}} &= \frac{\delta(\cos\theta - \cos\theta_1)}{2\pi (m_e c)^2 p\gamma} \frac{\partial \sigma_c^+}{\partial \gamma}(p, p_1), \\
\frac{\partial \sigma_\gamma^+}{\partial \boldsymbol{p}} &= \frac{\delta(\cos\theta - \cos\theta_k)}{2\pi (m_e c)^2 p\gamma} \frac{\partial \sigma_\gamma^+}{\partial \gamma}(p, k), \\
\frac{\partial \sigma_{\rm br}}{\partial \boldsymbol{k}} &= \frac{\delta(\cos\theta_k - \cos\theta_1)}{2\pi k^2} \frac{\partial \sigma_{\rm br}}{\partial k}(k, p_1),
\end{aligned} \tag{2.7}$$

where $\gamma = \sqrt{1 + (p/m_e c)^2}$ is the Lorentz factor. The angles θ, θ_1 and θ_k are the angles between the accelerating electric field $\boldsymbol{E}$ (or in a magnetized plasma the magnetic field $\boldsymbol{B}$) and $\boldsymbol{p}$, $\boldsymbol{p}_1$ and $\boldsymbol{k}$, respectively. With an axisymmetric runaway distribution $f_{\rm RE}(\boldsymbol{p}_1) = f_{\rm RE}(p_1, \cos\theta_1)$, we then obtain the approximated positron source term

$$S_{\rm pos}(\gamma, \cos\theta) = \frac{n_{\rm tot} Z_{\rm tot} m_e c^2}{p\gamma} \int_{\gamma+2}^{\infty} \mathrm{d}\gamma_1 \, (\gamma_1^2 - 1) \frac{\partial \sigma^+}{\partial \gamma} f_{\rm RE}(\gamma_1, \cos\theta), \tag{2.8}$$

where the effective cross section now takes the form

$$\frac{\partial \sigma^+}{\partial \gamma}(\gamma, \gamma_1) = \frac{\partial \sigma_c^+}{\partial \gamma}(\gamma, \gamma_1) + \frac{(Z_{\rm tot}+1)^2}{Z_{\rm tot}} t_{\rm ava} n_{\rm tot} c \int_{\gamma+1}^{\gamma_1 - 1} \mathrm{d}k \, \frac{\partial \sigma_\gamma^+}{\partial \gamma}(\gamma, k) \frac{\partial \sigma_{\rm br}}{\partial k}(k, \gamma_1), \tag{2.9}$$

depending only on the simpler integrated cross sections that are only differential in the energy of the outgoing particle of interest. In Eq. (2.8) it is explicit that positrons are only generated in the direction of the incident energetic electrons – the electron distribution is sampled at the same pitch angle as the source. Further details of the positron source term in the presence of an avalanching electron distribution are given in Appendix A, where we present the differential cross sections used as well as illustrate typical shapes of the source term in Eq. (2.8).

The annihilation source takes the simpler form

$$S_{\rm an}(\mathbf{p}) = -n_{\rm tot} v \sigma_{\rm an}(p) f_{\rm pos}(\mathbf{p}), \tag{2.10}$$

where $\sigma_{\rm an}$ is the cross section for free positron-electron two-quanta annihilation against stationary target electrons (Heitler 1954)

$$\sigma_{\rm an} = \frac{\pi r_0^2}{(p/m_e c)(\gamma+1)}\left[\frac{\gamma^2+4\gamma+1}{p/m_e c}\ln\left(\gamma+\frac{p}{m_e c}\right)-\gamma-3\right]. \tag{2.11}$$

2.1. *Relative importance of pair production by collisions and by photons*

A peculiar phenomenon occurs when considering pair production in the presence of a strong electric field, where the number of energetic electrons grows exponentially in time. Because there is a delay between the emission of photons and their subsequent pair production, if the electron population has time to grow by a significant amount during one such photon-pair-production time, the direct positron generation in collisions may contribute with a relatively larger production of pairs. We will now proceed to derive the threshold electric field above which pair production in collisions is dominant due to this effect.

In order to evaluate the pair-production source terms we need an expression for the runaway electron distribution. In a spatially uniform fully ionized plasma with constant electric field, when the runaway generation is dominated by the avalanche mechanism – i.e. by multiplication through large-angle collisions – it is given by (Fülöp *et al.* 2006)

$$\begin{aligned} f_{\rm RE}(p,\xi,t) &= \frac{n_{\rm RE}(t)A(p)}{2\pi m_e c\gamma_0 p^2}\frac{\exp\left[-\frac{\gamma}{\gamma_0}-A(p)(1+\xi)\right]}{1-e^{-2A}}, \\ A(p) &= \frac{E/E_c+1}{Z_{\rm tot}+1}\gamma, \\ n_{\rm RE}(t) &= n_{\rm RE}(0)e^{t/t_{\rm ava}}, \\ \gamma_0 &= c_Z\ln\Lambda. \end{aligned} \tag{2.12}$$

Our choice for A differs slightly from that in Ref. (Fülöp *et al.* 2006), however agrees in the limit $E \gg E_c$, $p \gg m_e c$ and $1+\xi \ll 1$ where the solution is expected to be valid, but is here generalized to also capture the near-threshold limit $E \to E_c$ (Lehtinen *et al.* 1999; Hesslow *et al.* 2018). When pitch-angle averaged, the electron distribution is given by

$$\mathcal{F}_{\rm RE}(p,t) = 2\pi\int_{-1}^{1} {\rm d}\xi\, f_{\rm RE}(p,\xi,t) = \frac{n_{\rm RE}(t)}{m_e c\gamma_0}e^{-\gamma/\gamma_0}, \tag{2.13}$$

where the average runaway energy is given by $\gamma_0 m_e c^2 \approx (c_Z \ln\Lambda/2)\,{\rm MeV}$, which is typically of the order of 10-30 MeV in most scenarios of interest.

The total number of pairs created per unit time and volume is obtained by integrating the positron source function (2.8) over all momenta, yielding

$$\frac{{\rm d}n_{\rm pair}}{{\rm d}t} = n_e Z_{\rm tot} m_e c^2 \int_3^\infty {\rm d}\gamma_1\, \sigma^+(\gamma_1)\mathcal{F}_{\rm RE}(\gamma_1) \equiv n_e n_{\rm RE} Z_{\rm tot}\langle v\sigma^+\rangle_{\rm RE}, \tag{2.14}$$

$$\begin{aligned} \sigma^+(\gamma_1) &= \int_1^{\gamma_1-2}\frac{\partial\sigma^+}{\partial\gamma}(\gamma,\gamma_1)\,{\rm d}\gamma, \\ \langle v\sigma^+\rangle_{\rm RE} &= \frac{1}{n_{\rm RE}}\int_{\sqrt{8}}^\infty {\rm d}p_1\, v_1\sigma^+(\gamma_1)\mathcal{F}_{\rm RE}(\gamma_1). \end{aligned} \tag{2.15}$$

With the analytic form of Eq. (2.13) for the electron distribution, the pair production rate defined by the above equations is characterized by the two integrals

$$\langle v\sigma_c^+\rangle_{\mathrm{RE}} = \frac{m_e c^2}{n_{\mathrm{RE}}}\int_3^\infty \mathrm{d}\gamma_1\, \sigma_c^+(\gamma_1)\mathcal{F}_{\mathrm{RE}}(\gamma_1) \approx \alpha^2 r_0^2 c\frac{\gamma_0 - 6.7}{15},$$
$$\langle v\sigma_\gamma\rangle_{\mathrm{RE}} = \frac{m_e c^2}{n_{\mathrm{RE}}}\int_3^\infty \mathrm{d}\gamma_1\, \mathcal{F}_{\mathrm{RE}}(\gamma_1)\int_2^{\gamma_1-1}\mathrm{d}k\,\sigma_\gamma^+(k)\frac{\partial\sigma_{\mathrm{br}}}{\partial k}(k,\,\gamma_1) \approx \alpha^2 r_0^4 c(2.6\gamma_0 - 14.8), \quad (2.16)$$

where $\sigma_\gamma^+ = \int_1^{k-1}(\partial\sigma_\gamma^+/\partial\gamma)\,\mathrm{d}\gamma$, and the approximate formulas are least-square fits on the interval of γ_0 between 20 and 80, giving a maximum error of 2.5%. Within an error of less than 3%, the second expression differs from the first by a constant factor $40.75r_0^2$, allowing the total pair production rate to be written

$$\frac{\mathrm{d}n_{\mathrm{pair}}}{\mathrm{d}t} \approx Z_{\mathrm{tot}}\alpha^2 n_e r_0^2 c\frac{\gamma_0 - 6.7}{15}\left(1 + 40.75\frac{(Z_{\mathrm{tot}}+1)^2}{Z_{\mathrm{tot}}}t_{\mathrm{ava}}n_e c r_0^2\right). \quad (2.17)$$

With $t_{\mathrm{ava}}n_e c r_0^2 = c_Z/[4\pi(E/E_c - 1)]$, it is clear that there is a threshold field $E = E_{\mathrm{pp}}(Z_{\mathrm{tot}})$ above which the collisional pair production (described by the first term) will be dominant. When c_Z is independent of E, this threshold field is given by

$$\frac{E_{\mathrm{pp}}}{E_c} - 1 = \frac{(1+Z_{\mathrm{tot}})^2}{Z_{\mathrm{tot}}}\frac{c_Z}{4\pi r_0^2}\frac{\int_3^\infty \mathrm{d}\gamma_1\, e^{-\gamma_1/\gamma_0}\int_2^{\gamma_1-1}\mathrm{d}k\,\sigma_\gamma^+(k)\frac{\partial\sigma_{\mathrm{br}}}{\partial k}(k,\,\gamma_1)}{\int_3^\infty \mathrm{d}\gamma_1\, e^{-\gamma_1/\gamma_0}\sigma_c^+(\gamma_1)}$$
$$\approx 3.25 c_Z\frac{(1+Z_{\mathrm{tot}})^2}{Z_{\mathrm{tot}}}. \quad (2.18)$$

When $Z_{\mathrm{tot}} = 1$, the threshold field is $E_{\mathrm{pp}} \approx 33E_c$, but grows rapidly with Z_{tot}. With an air-like $Z_{\mathrm{tot}} = 8$, one obtains $E_{\mathrm{pp}} \approx 120E_c$. Since electric fields are typically close to threshold during lightning discharges, positron production in such scenarios can be expected to be dominated by photon pair production. Although this has been assumed to be true in previous atmospheric runaway studies, the domain of validity of such an assumption has not been discussed.

In the above we assumed an infinitely large homogeneous system. When runaway acceleration occurs only over a finite distance of length L of constant background parameters, the threshold field calculated above is valid when $L \gg L_{\mathrm{ava}} = ct_{\mathrm{ava}}$, that is, when the system is significantly longer than one avalanche mean-free path. When this is not satisfied, i.e. when $L \lesssim L_{\mathrm{ava}}$, a threshold condition for the length of the system is obtained instead, taking the form

$$L_{\mathrm{pp}} \approx \frac{Z_{\mathrm{tot}}}{(1+Z_{\mathrm{tot}})^2}\frac{3\times 10^7\,\mathrm{m}}{n_e[10^{20}\,\mathrm{m}^{-3}]}. \quad (2.19)$$

When $L_{\mathrm{pp}} \lesssim L \lesssim L_{\mathrm{ava}}$, photon pair production will be the dominant positron-generation mechanism.

In the remainder of this work, we will focus on scenarios where either $E \gtrsim E_{\mathrm{pp}}$ or $L \lesssim L_{\mathrm{pp}}$, so that pair production by photons is negligible. This is typical of runaway scenarios in tokamaks, where $L/L_{\mathrm{pp}} \ll 10^{-5}$ due to the small size of the device.

2.2. *Distribution function of fast positrons*

Equipped with the kinetic equation for positrons in a runaway scenario, we can now characterize its solutions. When the electric field is sufficiently large for the average pitch angle to be small, typically well satisfied when $A = (E/E_c + 1)\gamma/(Z_{\mathrm{tot}} + 1) \gtrsim 1$, the distribution function of fast positrons can be readily calculated analytically. The kinetics are then essentially one-dimensional, with the pitch-angle dynamics playing a peripheral role in the evolution of the energy spectrum.

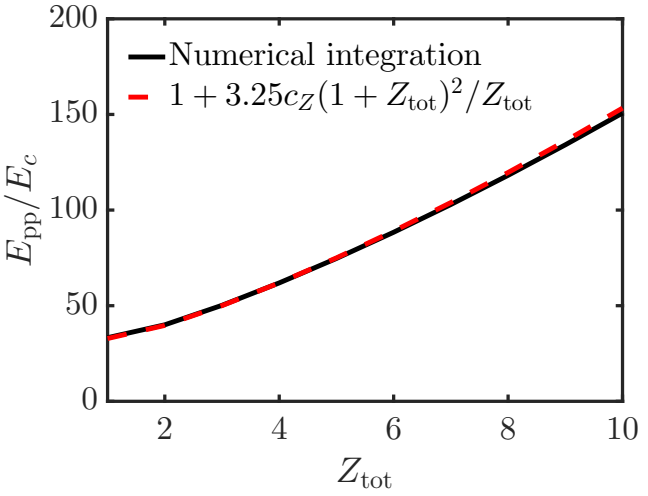

FIGURE 1. Critical field $E_{\rm pp}$ above which collisional positron production is the dominant pair-production mechanism in a uniform plasma, normalized to the avalanche threshold field E_c, calculated from the two expressions given in in Eq. (2.18) with $c_Z = \sqrt{5+Z_{\rm tot}}$.

We introduce a half-plane pitch-angle-averaged positron distribution function $\mathcal{F}$ as

$$\mathcal{F}(p) = 2\pi p^2 \times \begin{cases} \int_0^1 \mathrm{d}\xi\, f_{\rm RP}(p,\xi), & p \geqslant 0 \\ \int_{-1}^0 \mathrm{d}\xi\, f_{\rm RP}(|p|,\xi), & p < 0 \end{cases} \tag{2.20}$$

where the coordinate p now ranges from $-\infty$ to ∞. This distribution is defined so that $\int_{p_c}^\infty \mathcal{F}\,\mathrm{d}p = n_{\rm RP}$ equals the total runaway-positron density, with p_c a superthermal threshold in momentum distinguishing thermal positrons from runaways. In the same way, the thermal number density of positrons is $n_{\rm TP} = \int_{-p_c}^{p_c} \mathcal{F}\,\mathrm{d}p$.

In Appendix B we solve the positron kinetic equation (2.1) in the limit $(p/m_ec)^2 \gg 1$ assuming small pitch-angles $1-|\xi| \ll 1$. The resulting positron distribution is given by

$$\mathcal{F}(p) = \frac{Z_{\rm tot}}{4\pi \ln\Lambda r_0^2}\frac{n_{\rm RE}(t)}{\gamma_0 m_e c} e^{\rho\gamma/\gamma_0} \int_\gamma^\infty \mathrm{d}\gamma' \int_{\gamma'+2}^\infty \mathrm{d}\gamma_1 \frac{\partial\sigma^+}{\partial\gamma'}(\gamma',\gamma_1) \exp\left(-\frac{\rho\gamma'+\gamma_1}{\gamma_0}\right) \tag{2.21}$$

for $p < 0$, which describes the slowing-down distribution of the newly created positrons, where $\rho = (E/E_c - 1)/(E/E_c + 1)$, and

$$\mathcal{F}(p,t) = \frac{n_{\rm RP}(t)}{m_e c\gamma_0} e^{-\gamma/\gamma_0}, \tag{2.22}$$
$$n_{\rm RP}(t) = n_{\rm RP}(0) e^{t/t_{\rm ava}}$$

for $p > 0$, describing the runaway positron population that is undergoing acceleration in the electric field. Note that the prefactor, including the runaway-positron density evaluated at $t = 0$, is not determined in this derivation, but must instead be calculated in a more comprehensive kinetic equation accounting for the dynamics near $p \lesssim m_ec$.

We see that when $p > 0$, the runaway positron distribution satisfies $\mathcal{F}(p) = (n_{\rm RP}/n_{\rm RE})\mathcal{F}_{\rm RE}(-p)$. Indeed, for the full positron distribution, since the kinetic equation (2.1) is identical to the runaway-electron equation for $\xi > 0$ where the pair-production

source vanishes, we would expect

$$f_{\mathrm{RP}}(p,\,\xi,\,t) \approx \frac{n_{\mathrm{RP}}(t)}{n_{\mathrm{RE}}(t)} f_{\mathrm{RE}}(p,\,-\xi,\,t). \tag{2.23}$$

The expressions given above are valid for collisional as well as for photon pair-production during runaway scenarios.

We can now accurately evaluate the annihilation rate of runaway positrons, obtaining in the ultra-relativistic limit,

$$\begin{aligned}\frac{1}{\tau_{\mathrm{aR}}} = \frac{n_e}{n_{\mathrm{RP}}} \int_{p_c}^{\infty} \mathrm{d}p\, v\mathcal{F}(p)\sigma_{\mathrm{an}}(p) &\approx \frac{1}{4\ln\Lambda(E/E_c-1)t_{\mathrm{ava}}} \int_1^{\infty} \mathrm{d}\gamma \frac{\ln 2\gamma - 1}{\gamma} e^{-\gamma/\gamma_0} \\ &\approx \frac{\ln^2(\gamma_0/2.42)+1.55}{8\ln\Lambda(E/E_c-1)t_{\mathrm{ava}}},\end{aligned} \tag{2.24}$$

the final approximation having an error less than 2% for $\gamma_0 > 20$, and where the annihilation cross section σ_{an} was given in equation (2.11). We find that typically $t_{\mathrm{ava}}/\tau_{\mathrm{aR}} \lesssim 0.1/(E/E_c - 1)$, showing that annihilation has negligible impact on the avalanche-time-scale dynamics except for very close to the threshold field E_c. At that point, however, most of the created positrons will become thermalized, and only a negligible fraction will have time to annihilate before reaching thermal energies.

For $v \ll c$ the annihilation cross section takes the simple form $\sigma_{\mathrm{an}} \sim \pi r_0^2 c/v$, so that the thermal annihilation time τ_{aT} for a thermal positron population of temperature $T \ll 511\,\mathrm{keV}$ is given simply by

$$\frac{1}{\tau_{\mathrm{aT}}} = \pi n_e r_0^2 c = \frac{1}{4t_{\mathrm{ava}}} \frac{c_Z}{E/E_c - 1}. \tag{2.25}$$

In the presence of partially ionized or neutral gases, however, the cold positrons may annihilate also through the formation of positronium, which has significantly shorter, sub-μs lifetime. The annihilation time of thermal positrons is then rather set by the positronium formation rate, which is of the order of $n_i v a_0^2$, with a_0 the Bohr radius (Charlton & Humberston 2001).

2.3. *Numerical distribution function*

The positron Fokker-Planck equation, Eq. (2.1), can be solved as an initial value problem to give the evolution of the positron distribution function in the presence of an accelerating electric field. By adding the source and annihilation terms to the CODE (Landreman *et al.* 2014; Stahl *et al.* 2016) numerical kinetic solver, we calculate the distribution function for various electric fields and effective ion charges. CODE uses a continuum-spectral discretization scheme and has been used extensively to calculate runaway electron distributions including partial screening effects (Hesslow *et al.* 2017), synchrotron radiation (Stahl *et al.* 2015; Hirvijoki *et al.* 2015), bremsstrahlung (Embréus *et al.* 2016), and close collisions (Embréus *et al.* 2018).

Figure 2 illustrates the angle-averaged positron distribution for two cases: (*i*) with $E = 2E_c$ and $Z_{\mathrm{tot}} = 10$, and (*ii*) $E = 10E_c$ and $Z_{\mathrm{tot}} = 1$. The analytic solution, Eqs. (2.21) and (2.22), is nearly indistinguishable from the numerical solution for $p < 0$ for both cases, and for $p > 0$ in case (*ii*) with the higher electric field (shown in blue). The analytic solution fails to fully capture the low energy-behaviour in case (*i*) with low electric field and high plasma charge (black), where pitch-angle dynamics become important. The accuracy of the analytic solution at high electric field further motivates the neglect of annihilation in the dynamics of fast positrons. The sharp peaks at $p = 0$ in the numerical

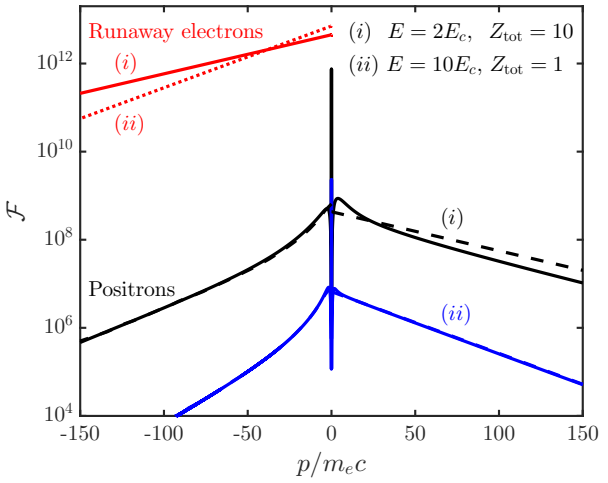

FIGURE 2. Pitch-angle averaged distribution functions $\mathcal{F}$ after 10 avalanche times $t_{\rm ava}$, with an initial runaway-electron density $n_{\rm RE,0} = 10^{10}\,{\rm m}^{-3}$, $n_e = 5 \times 10^{19}\,{\rm m}^{-3}$ and $T = 100\,{\rm eV}$. Runaway electrons in red and positrons in black and blue. Dashed lines denote the theoretical predictions of Eqs. (2.21) and (2.22); in the (ii) $E = 10E_c$, $Z_{\rm tot} = 1$ case it fully overlaps with the numerical solution.

positron energy spectra contain the thermalized positron populations, which we do not consider the detailed dynamics of here.

3. Rate equations for runaway positrons

From the kinetic description of Section 2 we can find a reduced set of fluid equations which govern the evolution of the number densities of runaway positrons as well as thermal positrons. We introduce the runaway positron density $n_{\rm RP}$ and thermal positron density $n_{\rm TP}$ in the same way as in the previous section. These then satisfy the equations

$$\frac{\partial n_{\rm RP}}{\partial t} = Z_{\rm tot} n_e n_{\rm RE} \kappa(E, Z_{\rm tot}) \langle v \sigma_c^+ \rangle_{\rm RE} - n_{\rm RP}/\tau_{\rm aR} \tag{3.1}$$

$$\frac{\partial n_{\rm TP}}{\partial t} = Z_{\rm tot} n_e n_{\rm RE} \eta(E, Z_{\rm tot}) \langle v \sigma_c^+ \rangle_{\rm RE} - n_{\rm TP}/\tau_{\rm aT} \tag{3.2}$$

$$\frac{\partial n_{\rm RE}}{\partial t} = n_{\rm RE} \Gamma_{\rm ava}(E, Z_{\rm tot}). \tag{3.3}$$

where κ denotes the fraction of created positrons that are accelerated as runaways, η the fraction that is thermalized, and $\Gamma_{\rm ava} = 1/t_{\rm ava}$ is the avalanche growth rate of runaway electrons.

Kinetic simulations must be used to determine the runaway fraction κ and thermalization fraction η (note that they will not sum to unity, since the population of fast newly-born positrons with $\xi < 0$ also grows in time). Results from numerical simulations for a variety of electric fields and plasma charges are shown in Fig. 3, obtained for constant electric fields and plasma charge. These are applicable to scenarios where E and $Z_{\rm tot}$ vary slowly in time compared to the avalanche time. When $E \gg E_c$, the runaway fraction is near unity, but decreases exponentially in magnitude when the electric field approaches the threshold value E_c. As only a small fraction of positrons are annihilated before slowing down (or entering the runaway region) (Heitler 1954), the effect of annihilation on the

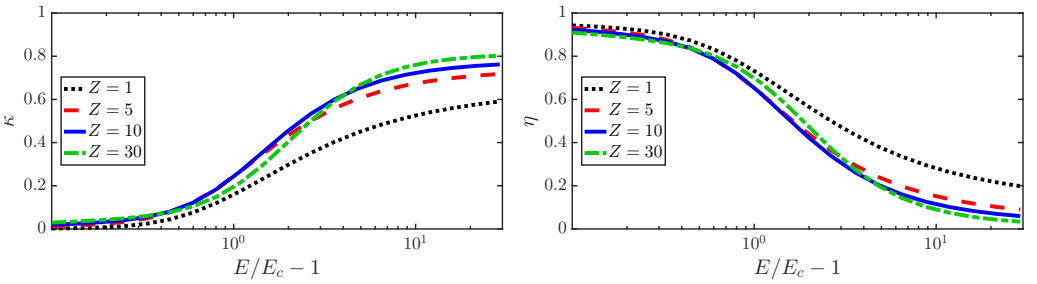

FIGURE 3. (left) Positron runaway fraction κ defined by Eq. (3.1), for various electric-field strengths and plasma effective charge $Z_{\rm tot}$. (right) Positron thermalization fraction η defined by Eq. (3.2), for various electric-field strengths and plasma effective charge $Z_{\rm tot}$.

positron-runaway-generation dynamics can be ignored, and we can assume that positrons are only annihilated after being either thermalized or runaway-accelerated.

In the presence of a constant electric field, background density and charge, the rate equations have a simple analytic solution given by (after a short transient phase on the scale of $t_{\rm ava}$)

$$\begin{aligned} n_{\rm RE}(t) &= n_0 \exp(\Gamma_{\rm ava} t), \\ n_{\rm RP}(t) &= n_{\rm RE}(t) \frac{Z_{\rm tot} \kappa n_e \langle v \sigma_c^+ \rangle}{\Gamma_{\rm ava} + \tau_{\rm aR}^{-1}}, \\ n_{\rm TP}(t) &= n_{\rm RE}(t) \frac{Z_{\rm tot} \eta n_e \langle v \sigma_c^+ \rangle}{\Gamma_{\rm ava} + \tau_{\rm aT}^{-1}}. \end{aligned} \tag{3.4}$$

Note that the positron populations grow in time despite annihilation; this occurs due to the ever-increasing amplitude of the positron source, since the runaway electrons are avalanching.

When the electric field is significantly above threshold one finds that $\Gamma_{\rm ava} \gg \tau_{\rm aR}^{-1}$ meaning that annihilation is negligible, so that

$$\frac{n_{\rm RP}}{n_{\rm RE}} \approx \frac{\kappa(E, Z_{\rm tot})}{E/E_c - 1} \frac{Z_{\rm tot} \langle v \sigma_c^+ \rangle}{4\pi c r_0^2 / c_Z} \approx \alpha^2 c_Z Z_{\rm tot} \frac{\kappa(E, Z_{\rm tot})}{E/E_c - 1} \frac{\gamma_0 - 6.7}{60\pi}, \tag{3.5}$$

where again $\gamma_0 = c_Z \ln \Lambda$. The electric-field dependence is fully captured in the factor $\kappa/(E/E_c - 1)$, which takes its maximal value ≈ 0.2 near $E \approx 2E_c$, only weakly dependent on the charge $Z_{\rm tot}$. With $\ln \Lambda = 15$, we then find that the maximal ratio of runaway positrons to electrons is $n_{\rm RP}/n_{\rm RE} \lesssim 8.5 \cdot 10^{-7} Z_{\rm tot} c_Z (c_Z - 0.45)$, which for a low-$Z$ plasma with $Z_{\rm tot} = 1$ is approximately $4{\times}10^{-6}$, and for a high-Z plasma with $Z_{\rm tot} = 20$ of the order of 4×10^{-4}. This means that the runaway-positron synchrotron and hard X-ray (HXR) emission may be challenging to distinguish from the radiation emitted by the runaway electrons in a tokamak, since even a small fraction of reflected or scattered radiation from electrons or noise from other sources could drown out the positron signal.

4. Radiation from positrons in tokamak plasmas

In the previous section we found that runaway positrons are less numerous than the runaway electrons by a factor smaller than approximately 10^{-4}. This causes a direct measurement of runaway positrons in a laboratory plasma to be challenging, and an appealing option is instead to detect the annihilation radiation of the positrons that have slowed down, which is distinctly peaked around photon energies of 511 keV. The

annihilation radiation from slow positrons is emitted approximately isotropically, whereas runaway electrons emit radiation primarily along their direction of motion, which when the electric field is large is along the electric field, or along the magnetic field in a magnetized plasma. This means that when measuring perpendicularly to the direction of runaway acceleration, even though the positrons are much fewer, their annihilation radiation may be detected through the X-ray background of runaway electrons for which only a small fraction is emitted at a $\pi/2$ angle and near 511 keV†. Furthermore, coincidence measurement techniques can be employed to carry out measurements in poor signal-to-noise ratio cases (Guanying *et al.* 2017).

We can make the heuristic discussion above stricter by the following arguments. The number density of bremsstrahlung photons emitted per unit solid angle, time and photon energy is given by

$$\frac{\partial n_{\mathrm{HXR}}}{\partial t \partial \Omega \partial k} = n_e Z_{\mathrm{tot}} \int_{\gamma > k+1} v \frac{\partial \sigma_{\mathrm{br}}}{\partial k \partial \Omega} f_{\mathrm{RE}}(\boldsymbol{p})\, \mathrm{d}\boldsymbol{p}. \tag{4.1}$$

This can be compared to the number density of annihilation photons emitted per unit time and solid angle due to the thermal positrons n_{TP} annihilating against the cold background,

$$\frac{\partial n_{\mathrm{an}}}{\partial t \partial \Omega} = \frac{n_{\mathrm{TP}}}{4\pi \tau_{\mathrm{aT}}} \approx Z_{\mathrm{tot}} \frac{n_{\mathrm{RE}} n_e \eta \langle v \sigma_c^+ \rangle_{\mathrm{RE}}}{4\pi}, \tag{4.2}$$

where we have assumed the thermal positron-annihilation rate to be much larger than the avalanche growth rate, $\Gamma_{\mathrm{ava}} \tau_{\mathrm{aT}} \ll 1$.

The annihilation radiation will have a line profile in photon energy with a characteristic width comparable to the background temperature. We consider the case where the profile is not resolved in the measurement, and the full line is captured in one channel. In this case, since the hard X-rays have a broad spectrum, we find it useful to characterize the visibility of the annihilation line with the parameter

$$\Delta k = \frac{\partial n_{\mathrm{an}} / \partial t \partial \Omega}{\partial n_{\mathrm{HXR}} / \partial t \partial \Omega \partial k}, \tag{4.3}$$

which (when $\Delta k \ll k$) can be interpreted as the photon-energy interval Δk around $k = m_e c^2$ within which the total HXR emission equals the annihilation photon flux. From a detection point of view, Δk would approximate the energy resolution required for the annihilation peak to appear with twice the amplitude of the continuous X-ray background. The finite line width of the annihilation peak would need to be accounted for when the plasma temperature satisfies $T \gtrsim \Delta k$.

In Fig. 4 we show Δk for detection at a $\pi/2$ angle relative to the direction of runaway acceleration, using the analytic runaway distribution of Eq. (2.12). We observe a relatively weak dependence on electric field where the main trend is approximately captured, within roughly 25%, by

$$\Delta k \approx \frac{7\,\mathrm{keV}}{\sqrt{Z_{\mathrm{tot}} + 1}}. \tag{4.4}$$

This means that in order for the annihilation peak to be clearly distinguishable from the X-ray background due to runaway electrons, an energy resolution better than or comparable to $(7/\sqrt{Z_{\mathrm{tot}} + 1})\,\mathrm{keV}$ is desirable. The contrast of X-rays to annihilation radiation, quantified through Δk, is largely insensitive to other parameters of the scenario,

† More precisely, the ratio of perpendicular to tangential bremsstrahlung emission is given by approximately $3/(8\gamma^4)$ at $k = 511\,\mathrm{keV}$.

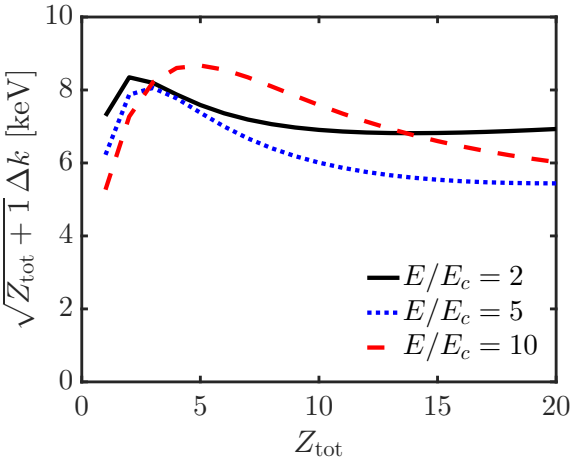

FIGURE 4. The photon-energy resolution parameter $\Delta k = (\partial n_{\rm an}/\partial t\partial\Omega)/(\partial n_{\rm HXR}/\partial t\partial\Omega\partial k)$ for perpendicular detection of annihilation radiation from thermalized positrons and hard X-rays from runaway electrons.

since the cross sections for the two processes scale in the same way with the background parameters.

There are two main competing effects which are sensitive to E and $Z_{\rm tot}$ that determine the observed behavior in Δk. When E increases, the thermalization fraction η of positrons rapidly decreases, as illustrated in Fig. 3 (right), which reduces the amount of 511 keV annihilation radiation. At the same time the runaway-electron population becomes more anisotropic, which sharply reduces the amount of bremsstrahlung emitted at a perpendicular angle. In the parameter range shown in the figure, these effects are found to approximately cancel, leaving only a weak E dependence. On the other hand, an increase in charge $Z_{\rm tot}$ causes the electron population to become more isotropic, *increasing* the amount of bremsstrahlung emitted at a perpendicular angle, however, it also increases the average runaway-electron energy which increases the number of positrons created per electron. The former effect is significantly stronger, which causes a net $1/\sqrt{Z_{\rm tot}+1}$ dependence.

Finally we note that, in the post-disruption runaway plateau where the runaway current slowly dissipates on the inductive time-scale of the device, the analytical avalanche runaway distribution that we have used here is not valid, as it tends to significantly overestimate the average energy of the distribution. Due to its experimental accessibility, we consider this scenario separately for a singly ionized argon-dominated plasma (Pautasso *et al.* 2016). For the runaway electron distribution we use the self-consistent slowing-down distribution of Ref. (Hesslow *et al.* 2018) obtained from a numerical solution of the kinetic equation with an inductive electric field and accurate modelling of screening effects on collisions, at a plasma temperature $T = 10\,\text{eV}$. Using such a numerical distribution function in evaluating the rate of pair production $\langle v\sigma_c^+\rangle_{\rm RE}$ and the bremsstrahlung photon flux yields $\Delta k = 0.31$ keV, which is approximately 20% of the value predicted by the rule-of-thumb given in Eq. (4.4) evaluated with $Z_{\rm tot} = 18$.

As well as being distinguishable from the runaway X-rays, it is required that the total number of annihilation photons reaching a detector is sufficiently large. While this is highly sensitive to the details of the setup, we can provide a rough estimate in the following way. The total number of annihilation photons per unit time reaching a detector

with area $A_{\rm det}$ placed a distance R from the plasma detecting emission within an opening angle $\Delta\theta$, is given approximately by

$$\begin{aligned}\frac{\partial N_{\rm an}}{\partial t} &\approx \Delta\theta \frac{A}{R} A_{\rm det} \frac{\partial n_{\rm an}}{\partial t \partial \Omega} \\ &\approx \Delta\theta A_{\rm det} A Z_{\rm tot} \frac{n_{\rm RE} n_e \eta \langle v \sigma_c^+ \rangle_{\rm RE}}{4\pi R} \\ &\approx \Delta\theta A_{\rm det} \frac{A n_{\rm RE} e c}{e} Z_{\rm tot} \frac{n_e r_0^2}{4\pi 137^2 R} \eta \frac{\gamma_0 - 6.7}{15} \\ &\approx (1.4 \times 10^6\,{\rm s}^{-1}) n_{20} I_{\rm RE}[100\,{\rm kA}] \times \\ &\quad \times \Delta\theta \frac{A_{\rm det}[{\rm dm}^2]}{R[{\rm m}]} Z_{\rm tot} (\gamma_0 - 6.7) \eta. \end{aligned} \tag{4.5}$$

Here, the cross-sectional area A of the plasma is assumed to be completely within the detector field-of-view. Then, discharges with higher plasma charge, background density and runaway current are seen to yield higher total annihilation-photon fluxes. Note that a strong decrease in total photon flux is found when the electric field increases above the threshold value E_c, due to the change in the thermalization fraction η. As an example, inserting values typical of a disruption in a medium-sized tokamak with $R = 1.5\,{\rm m}$, $Z_{\rm tot} = 10$, $n_{\rm tot} = 10^{20}\,{\rm m}^{-3}$, $I_{\rm RE} = 400\,{\rm kA}$, $E = 2E_c$, $A_{\rm det} = 1\,{\rm dm}^2$, $\Delta\theta = 0.5\,{\rm rad}$ and with $\ln\Lambda = 15$, one obtains a detected 511 keV annihilation photon count of $\partial N_{\rm an}/\partial t \approx 7 \times 10^8\,{\rm s}^{-1}$.

In poor signal-to-noise ratio cases coincidence measurements can be employed, where only positrons annihilated between two detectors are counted. This can be approximately accounted for in the previous formula by using an opening angle $\Delta\theta = \sqrt{A_{\rm det}}/R$ if two identical detectors are placed on either side of the plasma, which reduces the number of counts by another factor $0.1\,\sqrt{A_{\rm det}}[{\rm dm}]/R[{\rm m}]$.

5. Conclusions

Fast electrons can produce electron-positron pairs, primarily via either a two-step process based on the emission of a bremsstrahlung photon and a subsequent photon-particle interaction, or the direct process where pairs are produced in collisions between fast electrons and nuclei. We show that the former process is dominant when the electric field is above a certain threshold value, which is given in equation (2.18) and illustrated in Fig. 1. The latter process is however always dominant when the fast electrons are confined to a region in space which is smaller than the photon mean-free path, e.g. in magnetic fusion plasmas. Using a differential cross section for collisional pair production calculated using MadGraph 5 (Alwall *et al.* 2014), it is revealed that previous studies of pair production during runaway have significantly overestimated the positron generation rate.

In strong electric fields electrons and positrons are accelerated and may run away. The kinetic equations for electrons and positrons are similar, except for the opposite directions of acceleration in an electric field, and the source and annihilation terms present in the positron kinetic equation. We show that when the electric field is sufficiently large the positron distribution function can be calculated analytically, with explicit solutions given in Eqs. (2.21) and (2.22). The analytical solution shows remarkable agreement with numerical solutions of the kinetic equation in the relevant limit (high electric field and moderate charge number), as illustrated in Fig. 2.

Since the characteristic initial energy of the newly born positrons is large, a fluid description for the positron population can be used. Kinetic simulations are then only

needed to determine the fraction of created positrons that are thermalized or runaway-accelerated as a function of the background parameters. The evolution of the number density of thermal and runaway positrons can then be calculated from simple rate equations, given in Eqs. (3.1)-(3.3). These equations admit analytical solutions in the presence of a constant electric field, and can be used to determine the ratio of the runaway positron and electron populations. The runaway and thermalized positron fractions determined from numerical kinetic simulations are given for a variety of electric fields and charge numbers in Fig. 3.

Finally we calculate the radiation emitted by a positron population in a post-disruption tokamak plasma, and evaluate the annihilation to HXR ratio of photon fluxes emitted at a perpendicular angle to the system. Using these, one can estimate the parameter region where positrons can be detected, that is when their annihilation radiation is not overwhelmed by the bremsstrahlung radiation of energetic electrons and when the total photon count is sufficiently large.

The authors would like to thank G Ferretti and I Pusztai for fruitful discussions. This work was supported by the European Research Council (ERC-2014-CoG grant 647121) and the Swedish Research Council (Dnr. 2014-5510).

Appendix A. Positron source term

The differential cross sections appearing in Eq. (2.9) are given in the Born approximation by (Heitler 1954)

$$\begin{aligned}
\frac{\partial\sigma_\gamma^+}{\partial\gamma} &= \alpha r_0^2 \frac{pp_-}{k^3}\Bigg\{ -\frac{4}{3} - 2\gamma_-\gamma\frac{p_-^2+p^2}{p_-^2p^2} + \frac{\gamma}{p_-^3}\epsilon_- \\
&\quad + \frac{\gamma_-}{p^3}\epsilon - \frac{\epsilon_-\epsilon}{p_-p} + L_-\Bigg[k^2\frac{\gamma_-^2\gamma^2+p_-^2p^2}{p_-^3p^3} - \frac{8}{3}\frac{\gamma_-\gamma}{p_-p} \\
&\quad - \frac{k}{2p_-p}\Big(\frac{\gamma_-\gamma-p_-^2}{p_-^3}\epsilon_- + \frac{\gamma_-\gamma-p^2}{p^3}\epsilon + \frac{2k\gamma_-\gamma}{p_-^2p^2}\Big)\Bigg]\Bigg\}, \qquad \text{(A 1)} \\
\frac{\partial\sigma_{\mathrm{br}}}{\partial k} &= \alpha r_0^2 \frac{p}{kp_1}\Bigg\{\frac{4}{3} - 2\gamma_1\gamma\frac{p_1^2+p^2}{p_1^2p^2} + \epsilon_1\frac{\gamma}{p_1^3} + \epsilon\frac{\gamma_1}{p^3} - \frac{\epsilon_1\epsilon}{p_1p} \\
&\quad + L_1\Bigg[\frac{8}{3}\frac{\gamma_1\gamma}{p_1p} + k^2\frac{\gamma_1^2\gamma^2+p_1^2p^2}{p_1^3p^3} + \frac{k}{2p_1p}\Big(\epsilon_1\frac{\gamma_1\gamma+p_1^2}{p_1^3} \\
&\quad - \epsilon\frac{\gamma_1\gamma+p^2}{p^3} + 2k\frac{\gamma_1\gamma}{p_1^2p^2}\Big)\Bigg]\Bigg\}, \\
\epsilon &= 2\ln(\gamma+p) \qquad \text{(A 2)} \\
e\epsilon_1 &= 2\ln(\gamma_1+p_1) \\
\epsilon_- &= 2\ln(\gamma_-+p_-) \\
L_1 &= 2\ln\frac{\gamma_1\gamma+p_1p-1}{k}, \\
L_- &= 2\ln\frac{\gamma_-\gamma+p_-p-1}{k},
\end{aligned}$$

and $1/\alpha = 4\pi\varepsilon_0\hbar c/e^2 \approx 137$ denotes the inverse fine-structure constant. In the expression for $\partial\sigma_\gamma^+/\partial\gamma$, energy conservation constrains $\gamma_- = k - \gamma$ where $p_- = \sqrt{\gamma_-^2 - 1}$ denotes the momentum of the electron created in the pair, whereas in the expression for $\partial\sigma_{\mathrm{br}}/\partial k$ one

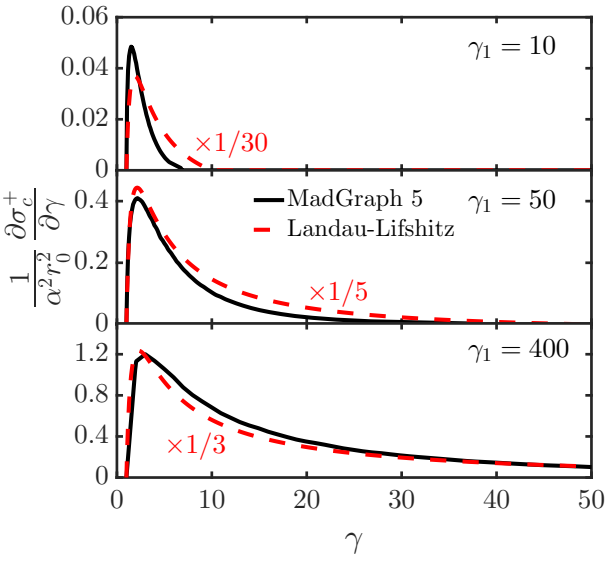

FIGURE 5. Differential cross section for pair production in collisions, by MadGraph 5 (solid black line, employed for results in this paper) and for comparison the Landau-Lifshitz formula (dashed red). γ_1 and γ are the incident-electron and outgoing-positron Lorentz factors, respectively. The Landau-Lifshitz formula has been multiplied by 1/30, 1/5 and 1/3 in the three subplots, respectively, in order to illustrate better the shapes of the curves. The MadGraph 5 results are significantly overestimated by the approximate formula.

has $\gamma = \gamma_1 - k$ and $p = \sqrt{\gamma^2 - 1}$ is the momentum of the outgoing positron. Here, momenta are expressed in units of $m_e c$ and k is the photon energy in units of $m_e c^2$.

The cross section $\partial\sigma_c^+/\partial\gamma$ for pair production in collisions by electrons and ions is evaluated in the Born approximation by the MadGraph 5 tool (Alwall *et al.* 2014), where 1,300,000 events were generated for each incident electron energy γ_1, for which 140 values between 3.13 and 587 were sampled (corresponding to a range from 1.6 MeV to 300 MeV). In Fig. 5 we compare $\partial\sigma_c^+/\partial\gamma$ as calculated by MadGraph 5 with the corresponding differential cross section evaluated in the main logarithmic approximation neglecting contributions of order $1/\ln\gamma_1$ (Landau & Lifshitz 1983),

$$\frac{\partial\sigma_{c,\mathrm{LL}}^+}{\partial\gamma} = \frac{56\alpha^2 r_0^2}{9\pi}\frac{\ln\gamma}{\gamma}\ln\frac{\gamma_1}{\gamma}. \tag{A 3}$$

We observe that the shape of the Landau-Lifshitz cross section $\mathrm{d}\sigma_{c,\mathrm{LL}}^+$ is qualitatively similar to the MadGraph 5 results, although the values deviate significantly from the more accurate calculation. At moderate-to-low electron energies, the Landau-Lifshitz formula also significantly overestimates the average positron energy. The disagreement between the Landau-Lifshitz formula and the corresponding Born approximation result is expected, since the logarithmic approximation is only valid at significantly higher energies than those relevant to runaway scenarios.

In Fig. 6 we compare the total pair production cross section σ_c^+ between MadGraph 5, the Landau-Lifshitz formula as well as with the formula given by Gryaznykh (1998),

$$\sigma_{c,\mathrm{Gr}}^+ = (5.11\,\mu\mathrm{b})\ln^3\frac{\gamma_1 + 3.6}{6.6}, \tag{A 4}$$

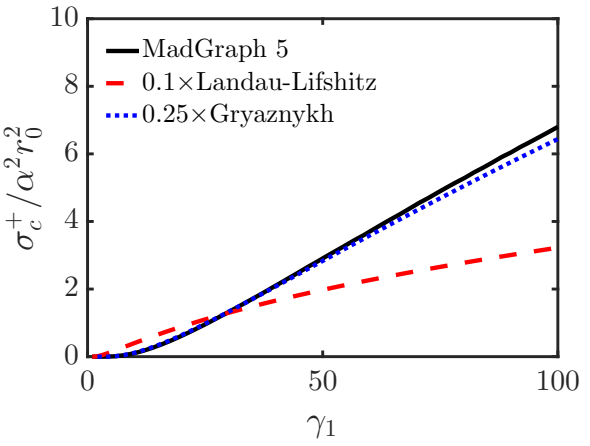

FIGURE 6. Total cross sections σ_c^+ by MadGraph 5 (solid, black), the Landau-Lifshitz formula (dashed, red) and the Gryaznykh formula (dotted, blue) as function of the incident-electron Lorentz factor γ_1. The Landau-Lifshitz and Gryaznykh formulas have been rescaled for better visibility; they both significantly overestimate the positron production compared to the full MadGraph 5 computation.

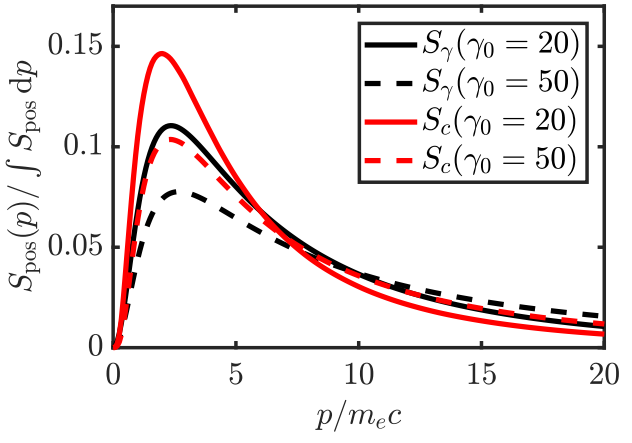

FIGURE 7. Positron source terms S_c (red), due to collisional pair production, and S_γ (black), due to pair production via X-ray emission, normalized to unity production rate, evaluated at different values of the average runaway energy $\gamma_0 = c_Z \ln\Lambda$. (solid, $\gamma_0 = 20$; dashed $\gamma_0 = 50$)

that has been employed in previous runaway positron studies. Although Gryaznykh's formula is a numerical fit to the full Born approximation result, it appears that the prefactor is too large by a factor of 4.

It is furthermore insightful to consider the energy spectrum of created positrons by integrating the positron source $S_{\rm pos}$ of Eq. (2.8) over angles,

$$S_{\rm pos}(p) = p^2 \int S_{\rm pos}(\boldsymbol{p})\,{\rm d}\Omega_{\boldsymbol{p}} = S_c(p) + S_\gamma(p), \tag{A 5}$$

where we have split the source into the contribution S_c from collisional pair production and S_γ from pair production via X-rays. These are defined so that $\int S_{\rm pos}\,{\rm d}p$ is the total rate at which positrons are produced, and are given explicitly by

$$S_c = n_e Z_{\rm tot} \nu \int_{\gamma+2}^{\infty} {\rm d}\gamma_1 \, \frac{\partial \sigma_c^+}{\partial \gamma} \mathcal{F}_{\rm RE}(\gamma_1), \tag{A 6}$$

$$S_\gamma = n_e^2 Z_{\rm tot} t_{\rm ava} \nu c \int_{\gamma+2}^{\infty} {\rm d}\gamma_1 \int_{\gamma+1}^{\gamma_1-1} {\rm d}k \, \frac{\partial \sigma_\gamma^+}{\partial \gamma} \frac{\partial \sigma_{\rm br}}{\partial k} \mathcal{F}_{\rm RE}(\gamma_1). \tag{A 7}$$

Figure 7 shows S_c and S_γ for two different systems, characterized by $\gamma_0 \equiv c_Z \ln\Lambda = 20$ and $\gamma_0 = 50$. It illustrates the dependence on the positron momentum p of the two pair production mechanisms, when averaged over the electron (and photon) distribution. It is clear that the two main pair-production channels due to runaway electrons – in collisions and via X-rays – produce very similar positron energy spectra.

We find that the average positron energy is not particularly sensitive to the average electron energy γ_0: by evaluating $\langle\gamma\rangle = \int_0^\infty \gamma S \, {\rm d}p / \int_0^\infty S \, {\rm d}p$, we obtain $\langle\gamma\rangle_c \approx 8$ and 11 when $\gamma_0 = 20$ and 50, respectively, for the collision term S_c. For the X-ray term S_γ we find $\langle\gamma\rangle_\gamma \approx 9$ and 13 for the corresponding cases. Energies of newly created positrons during runaway are therefore typically always in the 5 MeV range on average.

Appendix B. Derivation of positron distribution function

We here present the derivation of the positron distributions (2.21) and (2.22) in the high-energy, small-pitch-angle limit. The positron distribution varies over energies much larger than the rest energy, and thus satisfies the ultra-relativistic, one-dimensional kinetic equation

$$\frac{\partial \mathcal{F}(p,\,t)}{\partial t} + eE_c \left(\frac{E}{E_c} - {\rm sgn}(p) \right) \frac{\partial \mathcal{F}(p,\,t)}{\partial p} = n_e c Z_{\rm tot} \int_{\gamma+2}^{\infty} {\rm d}\gamma_1 \, \frac{\partial \sigma^+}{\partial \gamma}(\gamma,\,\gamma_1) \mathcal{F}_{\rm RE}(p_1,\,t), \tag{B 1}$$

where $p_1 = {\rm sgn}(p)\sqrt{\gamma_1^2 - 1}$. Here we have ignored the effect of annihilation on the evolution of the distribution, since this process occurs on a significantly longer time scale than the acceleration time in a strong electric field, and neglected the weak logarithmic energy dependence in the collisional friction force, taken to be constantly of magnitude $eE_c = m_e c/\tau_c$ with $\tau_c^{-1} = 4\pi \ln\Lambda n_e r_0^2 c$, opposing the direction of motion. We furthermore neglect radiation losses through synchrotron emission and bremsstrahlung; for high Z and low E, this assumption may be violated in the far tail of the energy distribution.

Since the electron population – which drives the generation of positrons through the pair-production source term – grows exponentially in time we expect the positron kinetic equation to have a quasi-steady-state solution of the form $\mathcal{F}(p,\,t) = e^{t/t_{\rm ava}} \mathcal{F}(p,\,0)$, growing at the same rate as the energetic electrons. For $p < 0$, the positron distribution then satisfies the first-order linear ODE

$$\left[\frac{E/E_c - 1}{\gamma_0} - \left(\frac{E}{E_c} + 1 \right) \frac{\partial}{\partial \gamma} \right] \mathcal{F} = \frac{Z_{\rm tot}}{4\pi \ln\Lambda r_0^2} \frac{n_{\rm RE}}{\gamma_0 m_e c} \int_\gamma^\infty {\rm d}\gamma_1 \, \frac{\partial \sigma^+}{\partial \gamma} e^{-\gamma_1/\gamma_0}, \tag{B 2}$$

where $\gamma_0 = c_Z \ln\Lambda$ is the average runaway-electron energy. Imposing the boundary condition $\mathcal{F}(-\infty,\,t) = 0$, thus constraining the solutions to a finite total positron number, it is solved by

$$\mathcal{F} = \frac{Z_{\rm tot}}{4\pi \ln\Lambda r_0^2} \frac{n_{\rm RE}}{\gamma_0 m_e c} e^{\rho\gamma/\gamma_0} \times \int_\gamma^\infty {\rm d}\gamma' \int_{\gamma'+2}^\infty {\rm d}\gamma_1 \left[\frac{\partial \sigma^+}{\partial \gamma'}(\gamma',\gamma_1) \exp\left\{ -\frac{\rho\gamma' + \gamma_1}{\gamma_0} \right\} \right] \tag{B 3}$$

where $\rho = (E/E_c - 1)/(E/E_c + 1)$.

Conversely, for $p > 0$, the pair-production source vanishes, and the positron distribution satisfies the same equation as the high-energy runaway electrons except for the opposite charge,

$$\frac{\partial \mathcal{F}}{\partial t} + eE_c\left(\frac{E}{E_c} - 1\right)\frac{\partial \mathcal{F}}{\partial p} = 0, \tag{B 4}$$

which is solved by

$$\mathcal{F}(p,t) = \mathcal{F}\left(0,\, t - \frac{p}{e(E-E_c)}\right). \tag{B 5}$$

Using as boundary condition at $p = 0$ that the positron population grows in time in the same way as the $p < 0$ population:

$$\frac{\mathcal{F}(0^+,\, t)}{\mathcal{F}(0^+,\, 0)} = \frac{\mathcal{F}(0^-,\, t)}{\mathcal{F}(0^-,\, 0)} = e^{t/t_{\mathrm{ava}}}, \tag{B 6}$$

which then immediately yields

$$\mathcal{F}(p,t) = \frac{n_{\mathrm{RP}}(0)}{m_e c \gamma_0} e^{t/t_{\mathrm{ava}}} e^{-\gamma/\gamma_0}. \tag{B 7}$$

REFERENCES

Alwall, J., Frederix, R., Frixione, S., Hirschi, V., Maltoni, F., Mattelaer, O., Shao, H.-S., Stelzer, T., Torrielli, P. & Zaro, M. 2014 The automated computation of tree-level and next-to-leading order differential cross sections, and their matching to parton shower simulations. *Journal of High Energy Physics* **7**, 79.

Anderson, C. D. 1932 The apparent existence of easily deflectable positives. *Science* **76** (1967), 238–239.

Briggs, M. S., Connaughton, V., Wilson-Hodge, C., Preece, R. D., Fishman, G. J., Kippen, R. M., Bhat, P. N., Paciesas, W. S., Chaplin, V. L., Meegan, C. A., von Kienlin, A., Greiner, J., Dwyer, J. R. & Smith, D. M. 2011 Electron-positron beams from terrestrial lightning observed with Fermi GBM. *Geophysical Research Letters* **38** (2), l02808.

Charlton, M. & Humberston, J. 2001 *Positron Physics*. Cambridge University Press.

Chen, H., Wilks, S. C., Bonlie, J. D., Liang, E. P., Myatt, J., Price, D. F., Meyerhofer, D. D. & Beiersdorfer, P. 2009 Relativistic positron creation using ultraintense short pulse lasers. *Phys. Rev. Lett.* **102**, 105001.

Connor, J. & Hastie, R. 1975 Relativistic limitations on runaway electrons. *Nuclear Fusion* **15**, 415.

Dreicer, H. 1959 Electron and ion runaway in a fully ionized gas I. *Physical Review* **115**, 238–249.

Dwyer, J. R. & Uman, M. A. 2014 The physics of lightning. *Physics Reports* **534** (4), 147 – 241.

Embréus, O., Stahl, A. & Fülöp, T. 2016 Effect of bremsstrahlung radiation emission on fast electrons in plasmas. *New Journal of Physics* **18** (9), 093023.

Embréus, O., Stahl, A. & Fülöp, T. 2018 On the relativistic large-angle electron collision operator for runaway avalanches in plasmas. *Journal of Plasma Physics* **84** (1), 905840102.

Ferretti, G. 2018 Private Communication.

Fülöp, T. & Papp, G. 2012 Runaway positrons in fusion plasmas. *Phys. Rev. Lett.* **108**, 225003.

Fülöp, T., Pokol, G., Helander, P. & Lisak, M. 2006 Destabilization of magnetosonic-whistler waves by a relativistic runaway beam. *Physics of Plasmas* **13** (6), 062506.

Gabrielse, G., Bowden, N. S., Oxley, P., Speck, A., Storry, C. H., Tan, J. N., Wessels, M., Grzonka, D., Oelert, W., Schepers, G., Sefzick, T., Walz, J., Pittner, H., Hänsch, T. W. & Hessels, E. A. 2002 Background-free observation of cold antihydrogen with field-ionization analysis of its states. *Phys. Rev. Lett.* **89**, 213401.

Gryaznykh, D. 1998 Cross section for the production of electron-positron pairs by electrons in the field of a nucleus. *Physics of Atomic Nuclei* **61** (3), 394–399.

Guanying, Y., Liu, J., Xie, J. & Li, J. 2017 Detection of tokamak plasma positrons using annihilation photons. *Fusion Engineering and Design* **118**, 124 – 128.

Gurevich, A. V. & Zybin, K. P. 2001 Runaway breakdown and electric discharges in thunderstorms. *Physics-Uspekhi* **44** (11), 1119–1140.

Haug, E. 1975 Bremsstrahlung and pair production in the field of free electrons. *Zeitschrift für Naturforschung A* **30** (9), 1099–1113.

Heitler, W. 1954 *The quantum theory of radiation*, , vol. 86. Courier Corporation.

Helander, P., Eriksson, L.-G. & Andersson, F. 2002 Runaway acceleration during magnetic reconnection in tokamaks. *Plasma Physics and Controlled Fusion* **44**, B247–62.

Helander, P. & Ward, D. J. 2003 Positron creation and annihilation in tokamak plasmas with runaway electrons. *Phys. Rev. Lett.* **90**, 135004.

Hesslow, L., Embréus, O., Stahl, A., DuBois, T. C., Papp, G., Newton, S. L. & Fülöp, T. 2017 Effect of partially screened nuclei on fast-electron dynamics. *Phys. Rev. Lett.* **118**, 255001.

Hesslow, L., Embréus, O., Wilkie, G. J., Papp, G. & Fülöp, T. 2018 Effect of partially ionized impurities and radiation on the effective critical electric field for runaway generation. *Plasma Phys. Controlled Fusion* .

Hirvijoki, E., Pusztai, I., Decker, J., Embréus, O., Stahl, A. & Fülöp, T. 2015 Radiation reaction induced non-monotonic features in runaway electron distributions. *Journal of Plasma Physics* **81** (5), 475810502.

Hollmann, E. M., Parks, P. B., Commaux, N., Eidietis, N. W., Moyer, R. A., Shiraki, D., Austin, M. E., Lasnier, C. J., Paz-Soldan, C. & Rudakov, D. L. 2015 Measurement of runaway electron energy distribution function during high-z gas injection into runaway electron plateaus in DIII-D. *Physics of Plasmas* **22** (5), 056108.

Hunt, A. W., Cassidy, D. B., Selim, F. A., Haakenaasen, R., Cowan, T. E., Howell, R. H., Lynn, K. G. & Golovchenko, J. A. 1999 Spatial sampling of crystal electrons by in-flight annihilation of fast positrons. *Nature* **402**, 157.

Jayakumar, R., Fleischmann, H. & Zweben, S. 1993 Collisional avalanche exponentiation of runaway electrons in electrified plasmas. *Physics Letters A* **172**, 447 – 451.

Landau, L. & Lifshitz, E. 1983 *Quantum electrodynamics*. Pergamon.

Landreman, M., Stahl, A. & Fülöp, T. 2014 Numerical calculation of the runaway electron distribution function and associated synchrotron emission. *Computer Physics Communications* **185** (3), 847 – 855.

Lehtinen, N. G., Bell, T. F. & Inan, U. S. 1999 Monte Carlo simulation of runaway MeV electron breakdown with application to red sprites and terrestrial gamma ray flashes. *Journal of Geophysical Research: Space Physics* **104** (A11), 24699.

Liu, C. & Wang, H. 2009 Reconnection electric field and hardness of X-Ray emission of solar flares. *The Astrophysical Journal* **696**, L27–L31.

Liu, J., Qin, H., Fisch, N. J., Teng, Q. & Wang, X. 2014 What is the fate of runaway positrons in tokamaks? *Physics of Plasmas* **21** (6), 064503, arXiv: https://doi.org/10.1063/1.4882435.

Murphy, R. J., Share, G. H., Skibo, J. G. & Kozlovsky, B. 2005 The physics of positron annihilation in the solar atmosphere. *The Astrophysical Journal Supplement Series* **161** (2), 495.

Pautasso, G., Bernert, M., Dibon, M., Duval, B., Dux, R., Fable, E., Fuchs, J., Conway, G., Giannone, L., Gude, A. & others 2016 Disruption mitigation by injection of small quantities of noble gas in ASDEX Upgrade. *Plasma Physics and Controlled Fusion* **59** (1), 014046.

Paz-Soldan, C., Cooper, C. M., Aleynikov, P., Pace, D. C., Eidietis, N. W., Brennan, D. P., Granetz, R. S., Hollmann, E. M., Liu, C., Lvovskiy, A., Moyer, R. A. & Shiraki, D. 2017 Spatiotemporal evolution of runaway electron momentum distributions in tokamaks. *Phys. Rev. Lett.* **118**, 255002.

Prantzos, N., Boehm, C., Bykov, A. M., Diehl, R., Ferrière, K., Guessoum, N., Jean, P., Knoedlseder, J., Marcowith, A., Moskalenko, I. V., Strong, A. &

Weidenspointner, G. 2011 The 511 keV emission from positron annihilation in the galaxy. *Rev. Mod. Phys.* **83**, 1001–1056.

Priest, E. & Forbes, T. 2002 The magnetic nature of solar flares. *The Astronomy and Astrophysics Review* **10** (4), 313–377.

Raichle, M. E. 1985 Positron emission tomography: Progress in brain imaging. *Nature* **317**, 574.

Rosenbluth, M. & Putvinski, S. 1997 Theory for avalanche of runaway electrons in tokamaks. *Nuclear Fusion* **37**, 1355–1362.

Sarri, G. 2015 Laser-driven generation of high-quality ultra-relativistic positron beams. *Journal of Plasma Physics* **81** (2).

Sokolov, Y. 1979 "multiplication" of accelerated electrons in a tokamak. *JETP Letters* **29**, 218–221.

Solodov, A. & Betti, R. 2008 Stopping power and range of energetic electrons in dense plasmas of fast-ignition fusion targets. *Physics of Plasmas* **15** (4), 042707.

Stahl, A., Embréus, O., Papp, G., Landreman, M. & Fülöp, T. 2016 Kinetic modelling of runaway electrons in dynamic scenarios. *Nuclear Fusion* **56** (11), 112009.

Stahl, A., Hirvijoki, E., Decker, J., Embréus, O. & Fülöp, T. 2015 Effective critical electric field for runaway electron generation. *Physical Review Letters* **114**, 115002.

Surko, C. M. & Greaves, R. G. 2004 Emerging science and technology of antimatter plasmas and trap-based beams. *Physics of Plasmas* **11** (5), 2333–2348.

Tsuchiya, H., Enoto, T., Yamada, S., Yuasa, T., Nakazawa, K., Kitaguchi, T., Kawaharada, M., Kokubun, M., Kato, H., Okano, M. & Makishima, K. 2011 Long-duration γ ray emissions from 2007 and 2008 winter thunderstorms. *Journal of Geophysical Research: Atmospheres* **116** (D9), d09113.

Wilks, S. C., Langdon, A. B., Cowan, T. E., Roth, M., Singh, M., Hatchett, S., Key, M. H., Pennington, D., MacKinnon, A. & Snavely, R. A. 2001 Energetic proton generation in ultra-intense laser-solid interactions. *Physics of Plasmas* **8** (2), 542–549.

Wilson, C. T. R. 1925 The acceleration of β-particles in strong electric fields such as those of thunderclouds. *Mathematical Proceedings of the Cambridge Philosophical Society* **22**, 534.